40 Gb/s VCSELs Test Data Collection, Analysis, and Process Problem Identification

Junyi Qiu, Hsiao-Lun Wang, Curtis Y. L. Wang, Xin Yu, and Milton Feng

Department of Electrical and Computer Engineering, University of Illinois at Urbana-Champaign,
Micro and Nanotechnology Laboratory, 208 N. Wright St., Urbana, IL 61801, U.S.A.
e-mail: mfeng@illinois.edu, Phone: +1 217-244-3662

Keywords: VCSEL, Testing, Data Analysis

Abstract

This paper reviews the on-wafer testing and subsequent data analysis procedures of 40 Gb/s oxide-confined VCSELs. Several key performance metrics are carefully defined and their measurement procedure explained. After data collection, a wafer-scale heat map is constructed to help to visualize device performance uniformity in terms of output power, threshold, and optical aperture diameter. Further data analysis reveals that the large variation of output power in this sample can be attributed to the VCSEL window quality, which is confirmed by reexamining the sample. Thus we have used VCSEL testing data analysis techniques to identify device processing issues, fully utilizing device testing as important quality assurance and information feedback step.

INTRODUCTION

Direct-modulated 850 nm oxide-confined VCSELs represent an optimum laser source for implementation of short-haul, high data rate and low power consumption optical interconnects. A record performance of 57 Gb/s error-free data transmission was recently demonstrated [1]. In this work we report the on-wafer DC and RF characterization of 40 Gb/s oxide-confined VCSELs, and the data analysis procedures that were developed to qualify the performance uniformity and identify possible issues occurred during the device fabrication process.

VCSEL TESTING PROCEDURE AND PERFORMANCE

The wafer is divided into four quadrants, each having 24 GS-layout (ground-signal layout probe pad) VCSEL singlets, 26 GS-layout 1x4 VCSEL arrays, and 8 GSG-layout (ground-signal-ground layout probe pad) singlets intended for RF characterization. First, the VCSEL RF performance is characterized by sample-testing the GSG singlets across the entire wafer. Out of a total of 32 GSG singlets, ten are then randomly picked to measure L-I-V curves, spectrum, and bandwidth. Due to the limited testing schedule, two of the ten are then selected to measure eye diagram and run Bit-Error-Rate Testing (BERT). These test results on the GSG devices serve as a preliminary wafer qualification step from which the best performing quadrant can be identified. This is then focused on for additional backend process. The DC performance (L-I-V and spectrum) is characterized by sample-testing 24 singlets and 16 1x4 arrays across the entire wafer. In total, 98 individual VCSELs (88 GS-layout and 10 GSG-layout) are measured and analyzed.

RF and the DC testing data are collected. In addition to optical output power (L) and lasing threshold (I_{th}), other important electrical and optical parameters are defined and characterized as well:

1) Optical aperture diameter is calculated from the mode spacing during the laser spectrum measurement by solving the cylindrical waveguide spatial confinement.
2) Chirp is measured by comparing the center emission wavelength with and without modulation.
3) Rise/fall time are read directly from the eye diagram measurement, which due to experiment setup includes both the VCSEL and the electrical components (bit-pattern generator, amplifier, probe, bias-T, fiber, photodetector, and oscilloscope). In order to extract the true VCSEL rise/fall time, one would strictly need to deconvolute all the other components' rise/fall times from the total amount, according to [2]:

$$T_R = (\sum_{1}^{n} {T_{Ri}}^2)^{1/2}$$

where T_{Ri} is the rise/fall time of the ith component and T_R is the total rise/fall time measured in the eye diagram. Alternatively, we use the "electrical eye" for a rough estimation of the total delay caused by non-VCSEL components, which is measured by directly looping the bit-pattern generator into the oscilloscope.
4) Optical modulation amplitude (OMA) can be obtained in two ways: the first approach is to calculate the optical output swing from the L-I-V curve based on the knowledge of the input differential impedance and the input voltage swing, and take into account of the impedance mismatch.

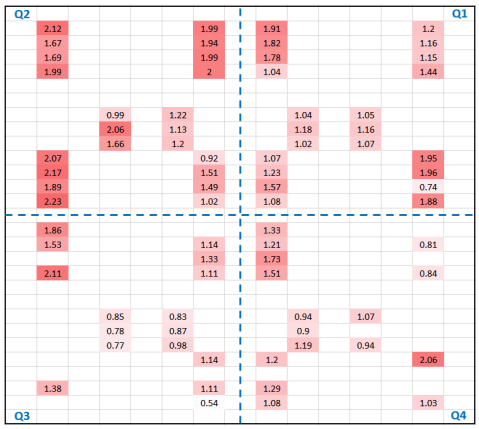

(a)

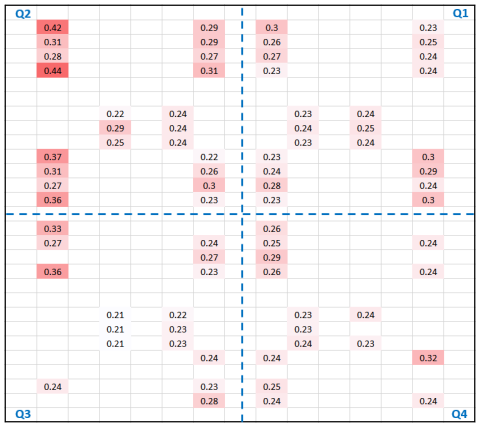

(b)

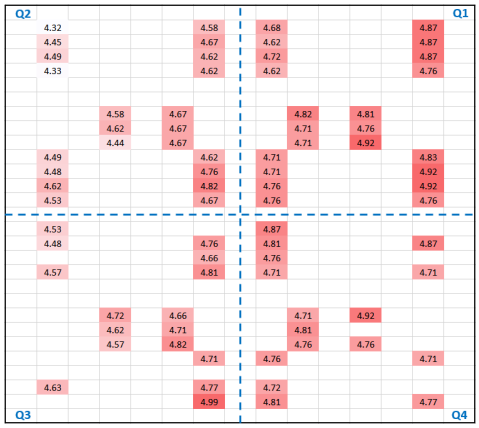

(c)

Fig. 1. Heat maps of the entire wafer showing the distribution of VCSEL parameters in terms of: (a) output power [mW], (b) threshold [mA], and (c) optical aperture diameter [um]. There appears to be a gradient from the upper-left corner (2nd quadrant) to the lower-right corner (4th quadrant).

This approach is computation-intensive because the VCSEL input impedance also varies with the bias current. The second approach is to directly measure the difference between the one-level and the zero-level in the eye diagram and divide it by the photodetector conversion gain. In our measurement these two approaches yield the same result.

5) Extinction ratio (ER) can be estimated from the OMA and the average power output by:

$$OMA = 2L_{avg}(\frac{ER-1}{ER+1})$$

where L_{avg} is the average output power roughly equal to the output power at the given bias point.

Based on (a) measured output power at given bias point (5 mA in this case), (b) threshold, and (c) optical aperture diameter, a wafer-scale heat map is constructed to illustrate the spatial uniformity of these device parameters (Fig. 1). Qualitatively, it is shown that devices near the upper-left corner (2nd quadrant) have higher output power, higher threshold, and slightly smaller optical aperture. In fact, the output power distribution shown in Fig. 1(a) has a standard deviation as high as 32% of the mean value, indicating a severe uniformity issue.

Data Collection, Analysis, and Process Problem Identification

The origin of this output power non-uniformity is analyzed below. The correlations between the output power and threshold, and between the output power and optical aperture diameter are plotted in Fig. 2. The output power appears to be strongly related to the threshold and very weakly related to the aperture size. Next, we refer to the laser output characteristic equation [3]:

$$L = \frac{1}{2}\frac{hv}{q}\eta_i\frac{\alpha_m}{\alpha_i+\alpha_m}(I-I_{th})$$

where L is the output power, $I = 5\ mA$ is the bias condition, and I_{th} is the threshold, α_i is the intrinsic loss, and α_m is the mirror loss. In fact, the above well-known equation can be derived from the Statz-DeMars rate equation [3,4]:

$$\frac{dN_{ph}}{dt} = v_g\Gamma g N_{ph} - \frac{N_{ph}}{\tau} = v_g\Gamma g N_{ph} - v_g(\alpha_i+\alpha_m)N_{ph}$$

where N_{ph} is the cavity photon density, v_g is the photon velocity, Γg is the modal gain, and τ is the cavity photon lifetime. The term $\frac{N_{ph}}{\tau}$ accounts for the total photon loss which is separated into intrinsic loss $v_g\alpha_i N_{ph}$ and mirror loss $v_g\alpha_m N_{ph}$. Thus the laser output can be expressed as:

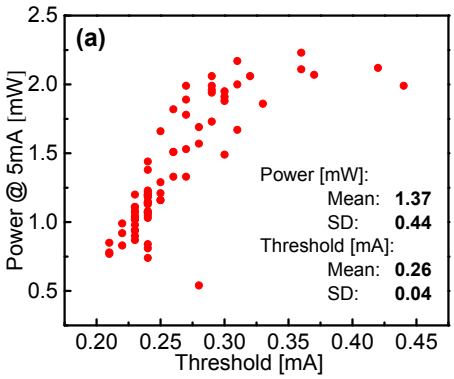

Fig. 2. Correlation plots of: (a) output power and threshold; (b) output power and optical aperture diameter. Each dot represents an individual VCSEL device. The output power distribution has a significantly larger standard deviation.

$$L = hv \cdot v_g \cdot \frac{1}{2}\alpha_m \cdot N_{ph}$$

The cavity photon density N_{ph} by assumption is proportional to $(\frac{I}{I_{th}} - 1)$, and with the fact that the laser threshold I_{th} is directly proportional to the total cavity loss $(\alpha_i + \alpha_m)$, we can derive the laser output characteristic equation. Thus it is clear the mirror loss α_m is directly proportional to $L/(\frac{I}{I_{th}} - 1)$. We can then plot L vs. $L/(\frac{I}{I_{th}} - 1)$ in Fig. 3(a) which is equivalent to L vs. α_m with arbitrary unit for the optical absorption coefficient. A clear dependence of the output power on the mirror loss is observed from the plot. The saturation towards the upper-right portion of the plot corresponds to the $\alpha_m/(\alpha_i + \alpha_m)$ factor in the laser output characteristic equation.

The I_{th} vs. $L/(\frac{I}{I_{th}} - 1)$ is also plotted in Fig. 3(b), which is equivalent to plotting I_{th} vs. $(\alpha_i + \alpha_m)$. Again a clear linear dependence is demonstrated which confirms the theory that $I_{th} \propto (\alpha_i + \alpha_m)$. Given the large variation of the

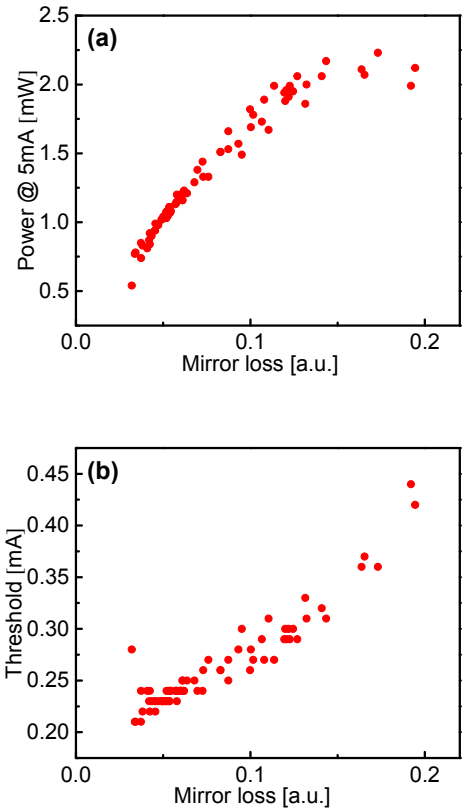

Fig. 3. After data analysis: (a) Plot of output power vs. mirror loss at arbitrary scale; a clear correlation is observed according to $L \propto \alpha_m/(\alpha_i + \alpha_m)$; (b) Plot of threshold vs. mirror loss at arbitrary scale; a clear linear trend is observed according to $I_{th} \propto (\alpha_i + \alpha_m)$. Thus the mirror quality is strongly affecting the device performance.

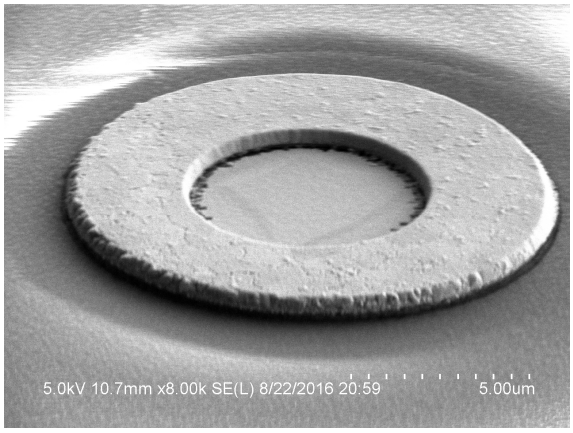

Fig. 4. SEM picture showing polymer residue on top of the VCSEL window, which possibly blocks light output and therefore reduces the mirror loss and the output power at given bias.

output power in contrast with the small variations of the threshold or the aperture size, it is reasonable to suggest that the quality of VCSEL window is the limiting factor to the device performance uniformity. It is likely that the devices near the lower-right corner are covered by polymer residue from previous processing steps, resulting in increased mirror reflectivity, reduced mirror loss, reduced threshold, and reduced output power at given bias, which would agree with the heat maps presented in Fig. 1. In fact, after reviewing the process steps, we identified possible polymer residue on top of the VCSEL window, shown in Fig. 4.

CONCLUSIONS

In conclusion, we have developed a high speed VCSEL device performance characterization procedure in which the key metrics are defined and explained. After data collection, a set of data analysis procedure is developed to correlate device parameters from which the performance-limiting factor can be identified and linked to potential device processing issues, fully utilizing the device testing step to provide feedbacks to the device processing step so that the device performance can keep improving.

ACKNOWLEDGEMENTS

We sincerely acknowledge the generous sponsorship of this research project by Foxconn Interconnect Technology (FIT) and guidance from Mr. Joe Liu and Dr. Ben Liaw. This work is supported in part by Dr. Michael Gerhold, Army Research Office (ARO) under Grant W911NF-17-1-0112, as well as Dr. Kenneth C. Goretta, Air Force of Scientific Research (AFOSR) under Grant FA9550-15-1-0122. Mr. Curtis Wang would like to thank the National Defense Science and Engineering Graduate (NDSEG) Fellowship for the support.

REFERENCES

[1] M. Liu, C. Y. Wang, M. Feng, and N. Holonyak, "Advanced Development of 850 nm Oxide-Confined VCSELs with a 57 Gb/s Error-Free Data Transmission," *GOMACTech-2016*, vol. 27.4, 2016.

[2] W. C. Elmore, "The transient response of damped linear networks with particular regard to wideband amplifiers," *J. Appl. Phys.*, vol. 19, no. 1, pp. 55–63, 1948.

[3] M. Feng, Junyi Qiu, C. Y. Wang and N. Holonyak, Jr. , "Intra-Cavity Photon-Assisted Tunneling Collector–Base Voltage Mediated Electro-Hole Spontaneous-Stimulated Recombination Transistor Laser," *J. Appl. Phys.*, vol. 119, 084502, 2016.

[4] H. Statz and G. DeMars, "Transients and oscillation pulses in masers," *Quantum Electronics*, pp. 530, 1960.

ACRONYMS

VCSEL: Heterojunction Bipolar Transistor
GS: Ground-Signal
GSG: Ground-Signal-Ground
BERT: Bit-Error-Rate Test
OMA: Optical Modulation Amplitude